Computers & Geosciences 35 (2009) 2100–2110

Contents lists available at ScienceDirect

Computers & Geosciences

journal homepage: www.elsevier.com/locate/cageo

Lacunarity analysis of raster datasets and 1D, 2D, and 3D point patterns ☆

Pinliang Dong *

Department of Geography, University of North Texas, 1155 Union Circle, #305279, Denton, TX 76203, USA

ARTICLE INFO

Article history:
Received 29 January 2007
Received in revised form
14 December 2008
Accepted 22 April 2009

Keywords:
Fractal
Scaling
Spatial modeling
Heterogeneity
GIS

ABSTRACT

Spatial scale plays an important role in many fields. As a scale-dependent measure for spatial heterogeneity, lacunarity describes the distribution of gaps within a set at multiple scales. In Earth science, environmental science, and ecology, lacunarity has been increasingly used for multiscale modeling of spatial patterns. This paper presents the development and implementation of a geographic information system (GIS) software extension for lacunarity analysis of raster datasets and 1D, 2D, and 3D point patterns. Depending on the application requirement, lacunarity analysis can be performed in two modes: global mode or local mode. The extension works for: (1) binary (1-bit) and grey-scale datasets in any raster format supported by ArcGIS and (2) 1D, 2D, and 3D point datasets as shapefiles or geodatabase feature classes. For more effective measurement of lacunarity for different patterns or processes in raster datasets, the extension allows users to define an area of interest (AOI) in four different ways, including using a polygon in an existing feature layer. Additionally, directionality can be taken into account when grey-scale datasets are used for local lacunarity analysis. The methodology and graphical user interface (GUI) are described. The application of the extension is demonstrated using both simulated and real datasets, including Brodatz texture images, a Spaceborne Imaging Radar (SIR-C) image, simulated 1D points on a drainage network, and 3D random and clustered point patterns. The options of lacunarity analysis and the effects of polyline arrangement on lacunarity of 1D points are also discussed. Results from sample data suggest that the lacunarity analysis extension can be used for efficient modeling of spatial patterns at multiple scales.

1. Introduction

The importance of spatial scale in many fields has led researchers to employ multiscale methods for spatial pattern analysis. For example, Vvedensky (2004) discussed multiscale modeling of nanostructures; Lucieer and Stein (2005) used a multiscale local binary pattern (LBP) operator to identify landform objects from a light detection and ranging (LiDAR) digital surface model (DSM); Lang et al. (2004) introduced a novel multiscale segmentation/object-relationship modeling method for better understanding of landscapes as hierarchies of patterns and processes; Hay et al. (2005) presented a multiscale object-specific segmentation (MOSS) approach for automatically delineating image objects; Watts et al. (2005) and Louie and Kolaczyk (2006) used multiscale methods to model the spread of diseases; Mygal and Phomin (2006) provided evidence of the multiscale spectral and spatial instabilities of the photoresponse in CdZnTe crystals. Dell'Acqua and Gamba (2006) used multiscale textural features from satellite Synthetic Aperture Radar (SAR) images for discriminating urban environments.

Mandelbrot (1982) introduced the concept of lacunarity to differentiate texture patterns that may have the same fractal dimension but appear strikingly different. Since the work by Mandelbrot (1982), lacunarity has been used as a scale-dependent measure for spatial patterns. Early methods for calculating lacunarity were given by Mandelbrot (1982), Gefen et al. (1984), Lin and Yang (1986), Voss (1986), and Allain and Cloitre (1991). Plotnick et al. (1993) used lacunarity as a measure of landscape texture. Plotnick et al. (1996) demonstrated that the concept of lacunarity can be extended to the description of spatial datasets, which may not necessarily be fractals. Dong (2000) proposed a new lacunarity estimation method for grey-scale image surfaces based on the gliding-box algorithm introduced by Allain and Cloitre (1991), and a differential box counting method in fractal dimension estimation proposed by Sarkar and Chaudhuri (1992). The method by Dong (2000) also included directionality when measuring lacunarity of image surfaces. In the last decade, lacunarity has been increasingly used for multiscale modeling of spatial patterns in Earth science, environmental science, and ecology. Examples include analysis of the temporal distribution of earthquakes (Xu and Burton, 1997), fragmentation and changes in hydrologic function of landscapes (Wu et al., 2000), spatial

☆The ArcGIS extension is available for free downloading from the website of the International Association of Mathematical Geosciences at www.iamg.org.

* Tel.: +1 940 565 2377; fax: +1 940 369 7550.
E-mail address: pdong@unt.edu

0098-3004/$ - see front matter © 2009 Elsevier Ltd. All rights reserved.
doi:10.1016/j.cageo.2009.04.001

characterization of sedimentation (Rankey, 2002), rock unit mapping (Dong and Leblon, 2004), simulation and quantification of forest canopy structure (Frazer et al., 2005; Malhi and Román-Cuesta, 2008), texture classification of urban areas (Myint and Lam, 2005), spatial pattern analysis of ecosystem (Wu et al., 2006), analysis of porosity in naturally fractured media (Miranda-Martinez et al., 2006), spatial modeling of water erosion (Vigiak et al., 2006), analysis of landscape fragmentation and ice storm damage (Pasher and King, 2006), and quantification of soil structure (Chun et al., 2008).

It has been noticed that many application examples of lacunarity analysis were based on binary raster data (0 and 1) representing the presence or absence of certain features. While grey-scale image data were used in some applications (for example, Henebry and Kux, 1995; Ranson and Sun, 1997; Malhi and Román-Cuesta, 2008), the images were normally converted into binary format prior to lacunarity analysis. This conversion may affect the accuracy of the results because of the loss of information when converting a grey-scale (for example 8-bit) image into a binary (1-bit) image. Moreover, many applications used datasets from a rectangular input area which may include: (1) a mixture of different spatial patterns and/or processes (for example, different land cover types), and (2) areas where no data is available. Therefore, it is essential to handle both binary and grey-scale image data and provide capabilities for users to define the area of interest (AOI) for lacunarity analysis. In a geographic information system (GIS), spatial data can be in raster format or vector format. In addition to raster images collected by remote sensing and geophysical methods, many data in Earth and environmental sciences have been collected as points in 1D (such as points along a drainage network or a transportation network), 2D (such as data from surface geochemical surveys), and 3D (such as 3D soil texture and structure, and LiDAR point clouds for vegetation canopies). Efficient analysis of spatial heterogeneity in 1D, 2D, and 3D points datasets is essential for many applications. This paper introduces the development of a lacunarity analysis extension for ArcGIS, a GIS software package developed by the Environmental Systems Research Institute (ESRI). Developed using Microsoft Visual Basic 6.0 and ESRI's ArcObjects 9.2, this extension works in Microsoft Windows operating systems to eliminate the above problems in lacunarity analysis, and provide a better environment for the integration of lacunarity-based multiscale modeling and spatial analysis in GIS. Following this introduction, Section 2 introduces the general flowchart for lacunarity analysis and major components of the methodology. Section 3 describes the implementation process and the graphical user interface. Examples are provided in Section 4, followed by discussions in Section 5 and conclusion in Section 6. The ArcGIS extension, user's guide, and sample data files can be downloaded from the website of the International Association of Mathematical Geosciences at www.iamg.org. Pseudo-codes for some major steps are listed in Appendices 1–3. A sample output text file is shown in Appendix 4.

2. Data and methodology

Fig. 1 shows the general flowchart for lacunarity analysis of raster (binary or grey-scale) and point (1D, 2D, and 3D) datasets. Details of data and methodology are described in the following sections.

2.1. Raster data

In some previous studies (Henebry and Kux, 1995; Ranson and Sun, 1997; Malhi and Román-Cuesta, 2008), grey-scale images (such as remotely sensed images) are generally converted to binary before lacunarity analysis, which may result in inaccurate spatial measurements. For example, two grey-scale images with different intensity surfaces can be converted to the same binary image using a proper threshold. In some other applications, data are presented in binary format (0 and 1) to show the presence or absence of certain features or phenomena. The Lacunarity Analysis extension works for both binary and grey-scale raster data in any format supported by ESRI's ArcGIS. Therefore,

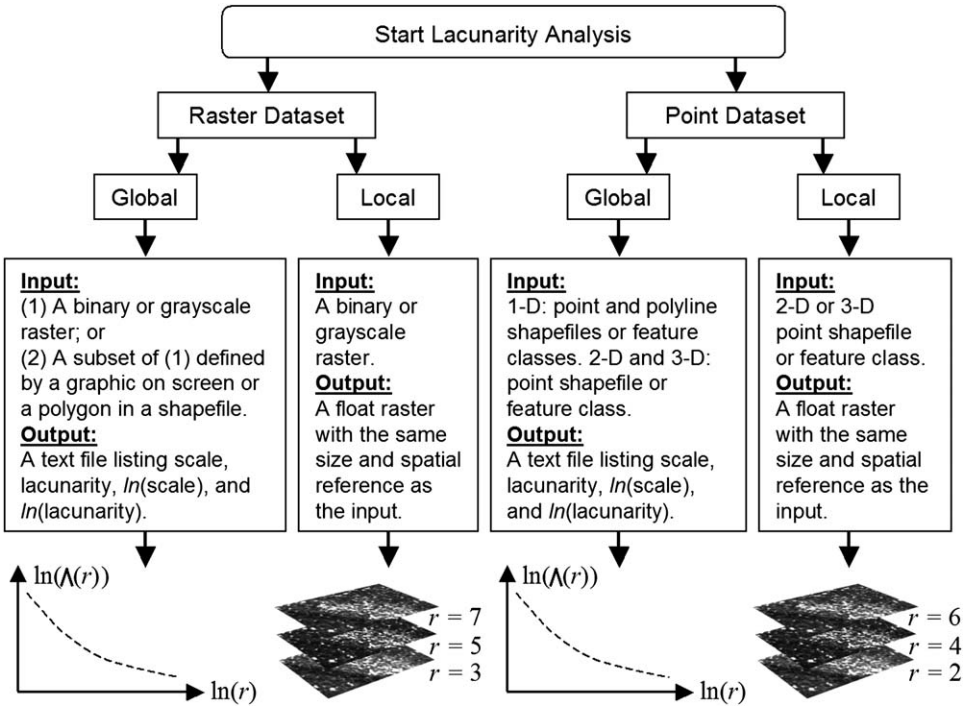

Fig. 1. Flowchart for lacunarity analysis extension.

grey-scale images do not have to be converted to binary for lacunarity analysis.

2.2. Point data

Points are a basic data type in GIS. Points can be collected for features or phenomena on one-dimensional networks, in two-dimensional areas, or in three-dimensional space. Point pattern analysis has been a research topic for decades (Boots and Getis, 1988; Ripley, 1988; Shoshany et al., 2007), and a thorough review of literature is beyond the scope of this paper. Here examples are presented to show the potential of lacunarity analysis for revealing point patterns (random, regular, or clustered) at multiple scales. A limited number of random point patterns are generated for comparison with clustered patterns. More intensive computer simulations may be required for more accurate characterization of point patterns in 1D, 2D, and 3D.

In raster format, the concept of pixel in 2D can be extended to 1D as linear pixel (lixel) and to 3D as volumetric pixel (voxel). Therefore, 1D, 2D, and 3D points can be converted into binary arrays depending on the presence or absence of point features (Fig. 2). The pseudo-code for generating a 1D array for points on a network is listed in Appendix 1. For 3D points, it should be noted that the voxel size in the Z direction can be different from that of the X and Y directions, and can be in a different unit of measurement. The range of Z values (floor to ceiling) can be specified so that only data points in the specified range can be used for analysis. For efficient conversion of 3D points to binary arrays, the points can be selected based on the size of voxels in the Z direction, and converted to raster bands layer by layer in a raster band collection. A 3D array is then obtained from the raster band collection for lacunarity analysis. This process is described in the pseudo-code in Appendix 1.

2.3. Lacunarity estimation

Lacunarity is a scale-dependent measure of heterogeneity (Gefen et al. 1984). Based on the analysis of the mass distribution in a deterministic or a random set, Allain and Cloitre (1991) proposed a gliding-box algorithm for lacunarity estimation. Consider a box of radius r that "glides" on a lattice overlaid on the set. If $n(M,r)$ is the number of gliding-boxes with radius r and mass M, the probability function $Q(M,r)$ is obtained by dividing $n(M,r)$ by the total number of boxes. The lacunarity at scale r is then defined by the mean-square deviation of the fluctuations of mass distribution probability $Q(M,r)$ divided by its square mean (Allain and Cloitre, 1991):

$$\Lambda(r) = \frac{\sum_M M^2 Q(M,r)}{\left[\sum_M M Q(M,r)\right]^2} \quad (1)$$

Lacunarity analysis of grey-scale images in this paper is based on a lacunarity estimation method developed by Dong (2000), using the gliding-box algorithm introduced by Allain and Cloitre (1991) and the differential box counting method in fractal dimension estimation proposed by Sarkar and Chaudhuri (1992). For lacunarity analysis of binary images, the gliding-box algorithm (Allain and Cloitre, 1991; Plotnick et al., 1993) is used. Detailed information on the algorithms can be found in these references.

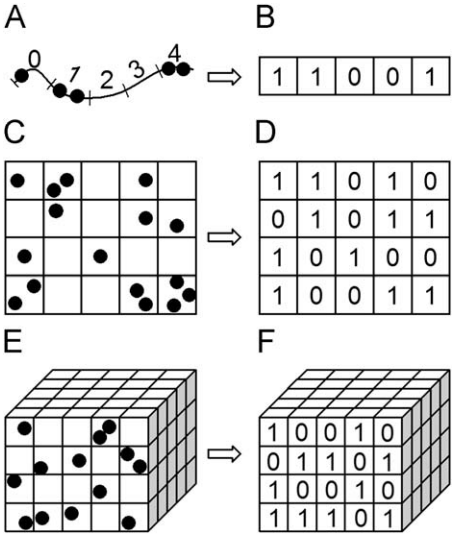

Fig. 2. Conversion of 1D, 2D, and 3D points into binary arrays.

2.4. Global lacunarity and local lacunarity

To meet the requirements of different applications, the extension was designed to calculate lacunarity in two different modes (Fig. 1): (1) global lacunarity—lacunarity values are calculated for the whole input raster dataset or an area of interest in the input dataset, and output as a text file listing lacunarity at different scales which can be imported into a graphic software for charting; (2) local lacunarity—lacunarity values are calculated from a window moving throughout the input dataset, and output as an float raster with the same size as the input raster dataset. ESRI's Spatial Analyst extension is required before lacunarity analysis can be conducted.

2.5. Moving-window, gliding-box, and partitioning of large datasets

For raster datasets and 2D point patterns, a moving-window ($w \times w$) moves throughout an input image, while a gliding-box ($r \times r$) moves throughout the moving-window. For global lacunarity, a moving-window is not needed, and the lacunarity of the input image at scale r, $\Lambda(r)$, is obtained after the gliding-box $r \times r$ moves throughout the image. For local lacunarity, the gliding-box $r \times r$ ($r < w$) moves throughout the moving-window $w \times w$, and the lacunarity $\Lambda(r)$ is calculated and assigned to the center of the moving-window. The moving-window then moves to the next location. For 1D and 3D point patterns, the gliding-box will be 1D and 3D, respectively. Table 1 lists the moving-window size and gliding-box size for raster datasets and point patterns. It should be noted that the moving-window for 3D point local lacunarity includes a Z dimension h, where h is the number of voxels in Z dimension.

If the input dataset (input raster or raster converted from points) is too big to be stored in computer memory, it needs to be partitioned into image blocks for processing. Generally, the gliding-box and the moving-window move with an increment of

Table 1
Moving-window size and gliding-box size for raster datasets and point patterns.

Dataset	Moving-window size		Gliding-box size	
	Global lacunarity	Local lacunarity	Global lacunarity	Local lacunarity
Raster (binary)	N/A	$w \times w$	$r \times r$	$r \times r$
Raster (grey-scale)	N/A	$w \times w$	$r \times r$	$r \times r$
1-D point pattern	N/A	N/A	r	N/A
2-D point pattern	N/A	$w \times w$	$r \times r$	$r \times r$
3-D point pattern	N/A	$w \times w \times h$	$r \times r \times r$	$r \times r \times r$

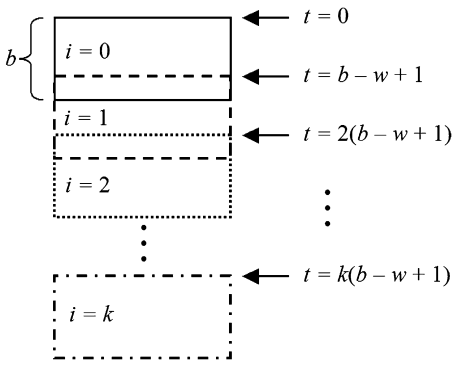

Fig. 3. Partitioning of input image into blocks. b is the block height, i is the block index, w is the moving-window size (odd integer), and t is the top offset of the block. Overlapping blocks are required in order to produce continuous output pixels in the output image.

one pixel, whereas the image block moves to a new location with some overlap with the previous block. Such an overlap is necessary because the effects of gliding-box size (for global lacunarity) or moving-window size (for local lacunarity) at the edges should be taken into account.

Suppose b is the height of the first block (solid box, $i = 0$) with a top offset $t = 0$ (Fig. 3). When all moving-windows sized $w \times w$ are processed, the second block (dashed box, $i = 1$) will be read in the memory. To ensure that a continuous output raster is produced, there will be an overlap between the first and second blocks. Therefore, the top offset of the second block is calculated as $t = b-w+1$. This process is repeated until the block reaches the bottom of the input raster. The height of the last block will be adjusted based on the moving-window size. Fig. 3 illustrates the calculation of top offsets for the overlapping blocks. The pseudo-code for lacunarity analysis of large datasets is listed in Appendix 3.

2.6. No data and area of interest

If the input raster contains areas where no data is available, these areas should be excluded during the process of lacunarity calculation. This extension takes into account No Data values to ensure that valid measurements can be made for the input raster. For global lacunarity analysis, the extension also allows the user to define an area of interest in four different ways: (1) define a rectangular area using the coordinates of the upper-left corner and the lower-right corner of the AOI; (2) draw a rectangle on screen; (3) draw a polygon on screen; and (4) use a selected polygon in a feature class. These options are listed on the graphical user interface (GUI) in Section 3.2, and examples are shown in Section 4.

2.7. Directionality

By default, directionality is not taken into account when calculating lacunarity of input datasets. As proposed in Dong (2000), directionality of lacunarity can be defined in four directions (0° for east–west direction, 45° for northeast–southwest direction, 90° for north–south direction, and 135° for northwest–southeast direction), and can provide useful information on grey-scale surfaces. These options for directionality are included in the extension for local lacunarity analysis of grey-scale image data.

3. Implementation

3.1. Project components

ESRI's ArcObjects are software components built with C++ for GIS application development. New GIS functionality can be added to ArcGIS with several choices of customization, and extensions provide the developer with a powerful mechanism for extending the core functionality of ArcGIS applications (ESRI, 2004). The lacunarity analysis extension was developed using Microsoft Visual Basic 6.0 and ESRI's ArcObjects 9.2. A Dynamic Link Library (DLL) file was compiled from a Visual Basic ActiveX project. The DLL file can be deployed to user's computer with other relevant files. Table 2 lists the components of the DLL project and major interfaces.

3.2. Graphic user interface

The GUI has three taps: Raster (global), Raster (local), and Points, as shown in Figs. 4–6. In the Raster (global) panel (Fig. 4), the user can select a binary or grey-scale raster as input. By default, lacunarity analysis is based on the whole input raster, but the user can define an area of interest using one of the four ways. The maximum gliding-box size is the maximum scale for lacunarity calculation. For example, if the maximum gliding-box size is 15×15, the lacunarity $\Lambda(r)$ will be calculated at

Table 2
Components of visual basic activex DLL project for lacunarity analysis.

Forms	frmLacunarity.frm
Modules	FunctionModules.bas
Class modules	Extension.cls (Implements: IExtension, IExtensionConfig)
	Help.cls (Implements: ICommand)
	DrawPolygon.cls (Implements: ICommand, ITool)
	DrawRectangle.cls (Implements: ICommand, ITool)
	StartLacunarity.cls (Implements: ICommand)
	Toolbar.cls (Implements: IToolbarDef)
Related documents	Lacunarity.res (resource file)

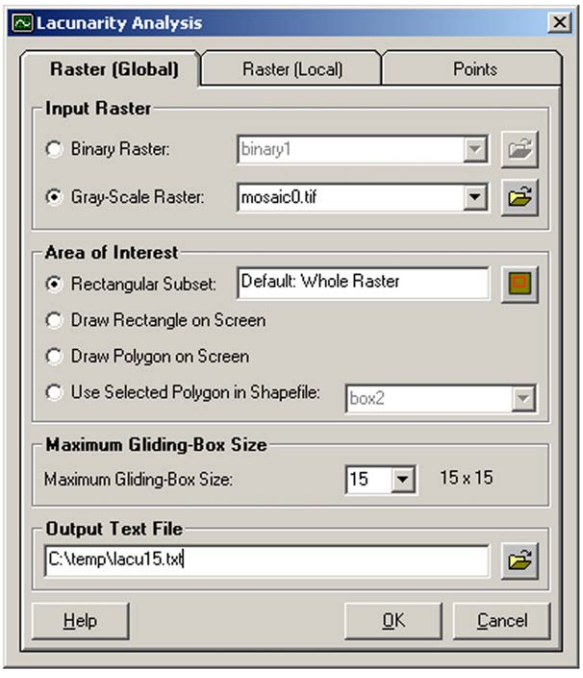

Fig. 4. Graphical user interface for global lacunarity analysis of rasters.

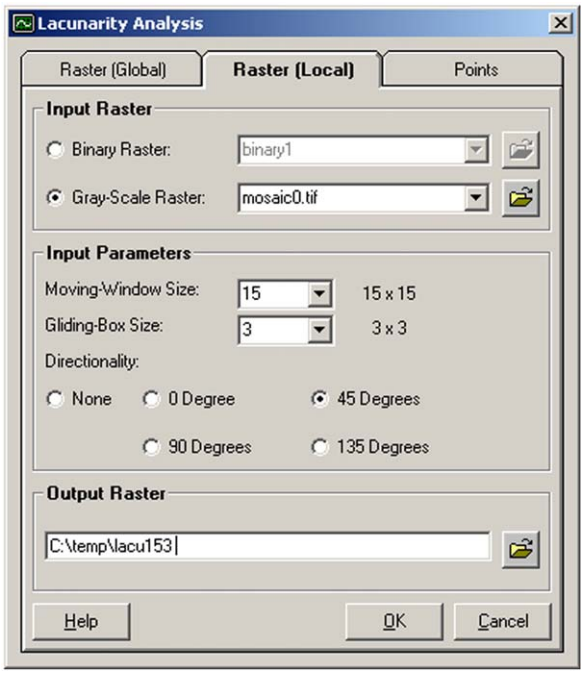

Fig. 5. Graphical user interface for local lacunarity analysis of rasters.

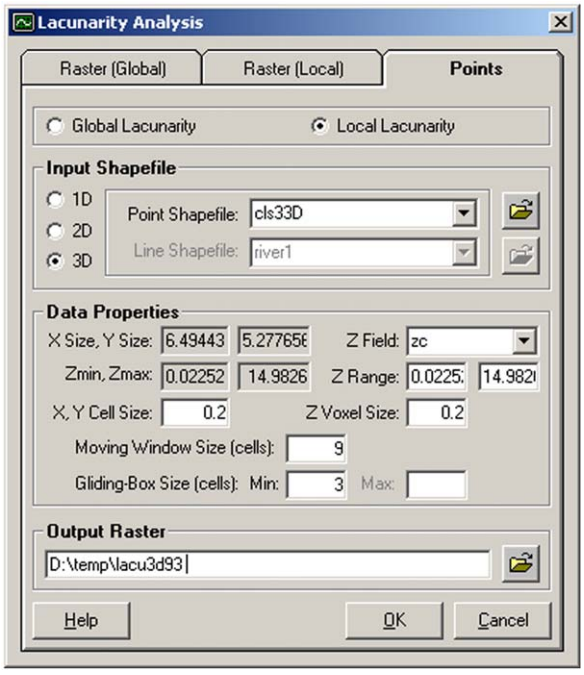

Fig. 6. Graphical user interface for global and local lacunarity analysis of points.

$r = 1,2,3,4,\ldots,15$ for binary rasters, and $r = 2,3,4,\ldots,15$ for grey-scale rasters. The output text file has four columns for scale, lacunarity, ln(scale), and ln(lacunarity). A sample output text file is attached in Appendix 4. The text file can be imported into a graphics program (such as Microsoft Excel) to create charts (see Section 4 for examples).

Fig. 5 shows the GUI for local lacunarity analysis of rasters. After specifying the input raster, moving-window size, and gliding-box size, the user can choose a directionality option. The output raster is an ESRI float grid dataset, which can be added to ArcMap after completion of the program. When the user clicks the "Help" button, A help document will be displayed using the default web browser of the computer (Internet connection is not required).

Fig. 6 is the GUI for global and local lacunarity analysis of 1D, 2D, and 3D points. For 1D points, a point shapefile and a line shapefile should be provided, and the points should be on the lines exactly. For 2D and 3D points, only a point shapefile can be used as input. The dimension (X Size, Y Size) of the input dataset will be shown. The user will specify output raster cell size, moving-window size (for local lacunarity), and gliding-box size. If 3D points are used as input, the user can select a Z field, and the minimum and maximum Z values (Z_{min}, Z_{max}) will be shown. By default, the Z range will be from Z_{min} to Z_{max}, but the user can use a different range and specify the voxel size in the Z direction. For global lacunarity analysis, the output is a text file, whereas a float gird dataset will be produced for local lacunarity analysis.

4. Examples

4.1. Results from binary patterns

Fig. 7 shows four binary images derived from the grey-scale Brodatz texture images (Brodatz, 1966) using random threshold values. Areas of interest are also shown on each image. Each image has 200×200 pixels, denoted by P1 (Fig. 7A), P2 (Fig. 7B), P3 (Fig. 7C), and P4 (Fig. 7D). These texture patterns have been widely used in evaluating computer vision and pattern recognition algorithms by many researchers. The lacunarity curves for the binary patterns and AOI's are shown in Fig. 8A and B, respectively. It can be seen that P3 has higher lacunarity at small scales (gliding-box sizes), which means the spatial arrangement of gaps in P3 is more heterogeneous compared with other patterns. Similarly, P1 has lower lacunarity values and is less heterogeneous compared with other patterns. In addition, Figs. 8A and B are very similar to each other, which suggests that areas of interest can be used to represent the whole spatial pattern for comparison of lacunarity values.

4.2. Results from grey-scale patterns

Fig. 9 shows lacunarity images obtained from a mosaic of four Brodatz texture patterns using gliding-box size $r = 3$ and moving-window size $w = 19$ with different directionality options. It can be seen that directionality can be very useful in separating the patterns. For example, P1 can be discriminated from the other patterns at 45° (Fig. 9C), while P3 is highlighted at 135° (Fig. 9D).

Similar results can be obtained from the L-band HH-polarization radar image in Pishan, Xinjiang, China, acquired by the Spaceborne Imaging Radar-C (SIR-C) aboard the space shuttle Endeavour in April 1994 (Fig. 10A). The image has been used by geologists to study past climate changes, volcanoes, and tectonics of the area (Guo et al., 1997). Ancient alluvial fans and gravel deposits formed during times of wetter climate. Continued plate–tectonic collision caused the uplift of Kunlun Mountains, and the ancient alluvial fans were cut into north–south tending valleys during the development of modern alluvial fans. As a result, ancient and modern alluvial fans show different texture patterns on this image. The contrast between the two texture patterns is enhanced when the direction of lacunarity analysis is 0° (Fig. 10C), perpendicular to the trending of the valleys in the ancient alluvial fans.

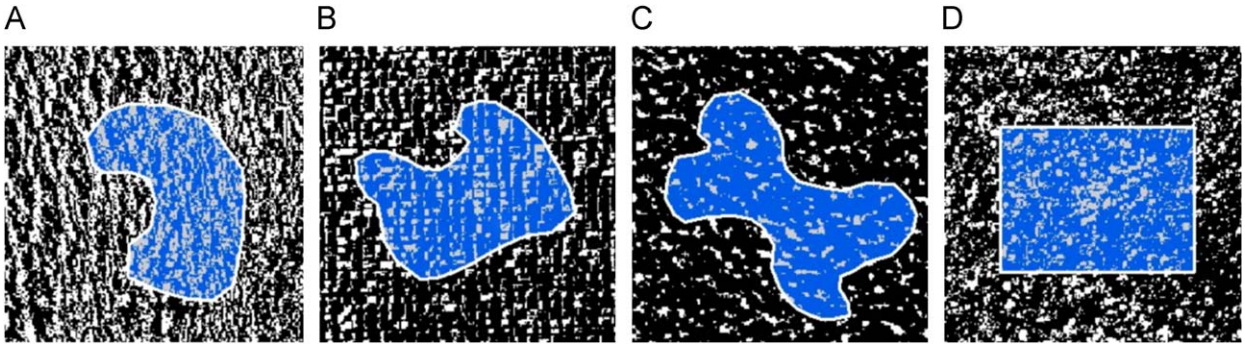

Fig. 7. Four binary patterns derived from Brodatz textures, with an area of interest on each pattern.

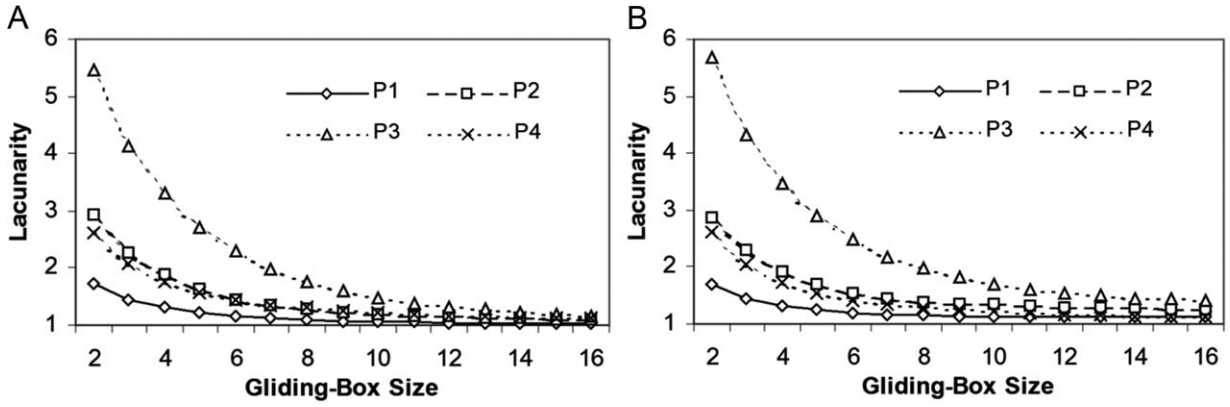

Fig. 8. (A) Lacunarity curves for binary patterns in Fig. 7. (B) Lacunarity curves for areas of interest in Fig. 7.

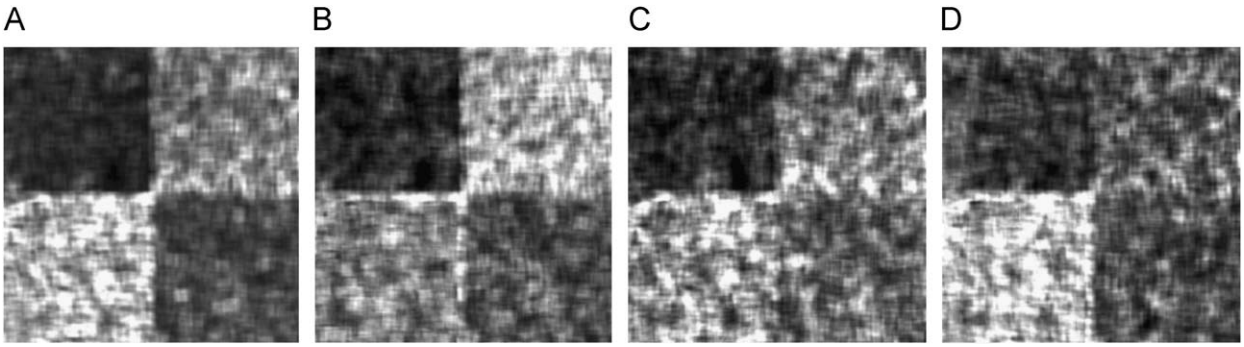

Fig. 9. Lacunarity images of four Brodatz texture patterns with different directionality options ($r = 3$, $w = 19$). (A) Non-Directional, (B) 0 Degree, (C) 45 Degrees and (D) 135 Degrees.

4.3. Results from point data

Fig. 11A shows 200 simulated 1D random points on a drainage system. In Fig. 11B, the total number of points is still 200, but the drainage branches inside the ellipses have 80 random points while the rest branches have 120 random points, thereby creating two-point clusters on the drainage system. Similar to Fig. 11B, Fig. 11C shows the same drainage branches with point clusters, but the number of points inside the ellipses increased to 120, whereas the number of points on the rest drainage branches reduced to 80. Lacunarity analysis results of the 1D point patterns are shown in Fig. 13A. Several random patterns with 200 points on the drainage system are also generated, and all of them show almost identical lacunarity curves (not shown here). This is expected because the gap size distributions of the random patterns should be very close to each other. From Fig. 13A it can be seen that the lacunarity of clustered patterns are higher than that of the random pattern, and that the more points on the branches inside the ellipses, the higher the lacunarity values at different scales. This can be explained by the fact that there are greater variations of gap sizes on the drainage when points are becoming more crowded on the branches inside the ellipses, and less crowded on the rest branches. Therefore, lacunarity can be used to test if a point pattern is random or clustered, and quantify the spatial heterogeneity of patterns at multiple scales.

Fig. 12A shows 1000 simulated random points in 3D space. The number of points remains unchanged, but the points start to form 4 clusters (Fig. 12B), 2 clusters (Fig. 12C), and 1 cluster (Fig. 12D). The lacunarity curves for the 3D random and clustered point patterns are shown in Fig. 13B. Similar to the results from 1D

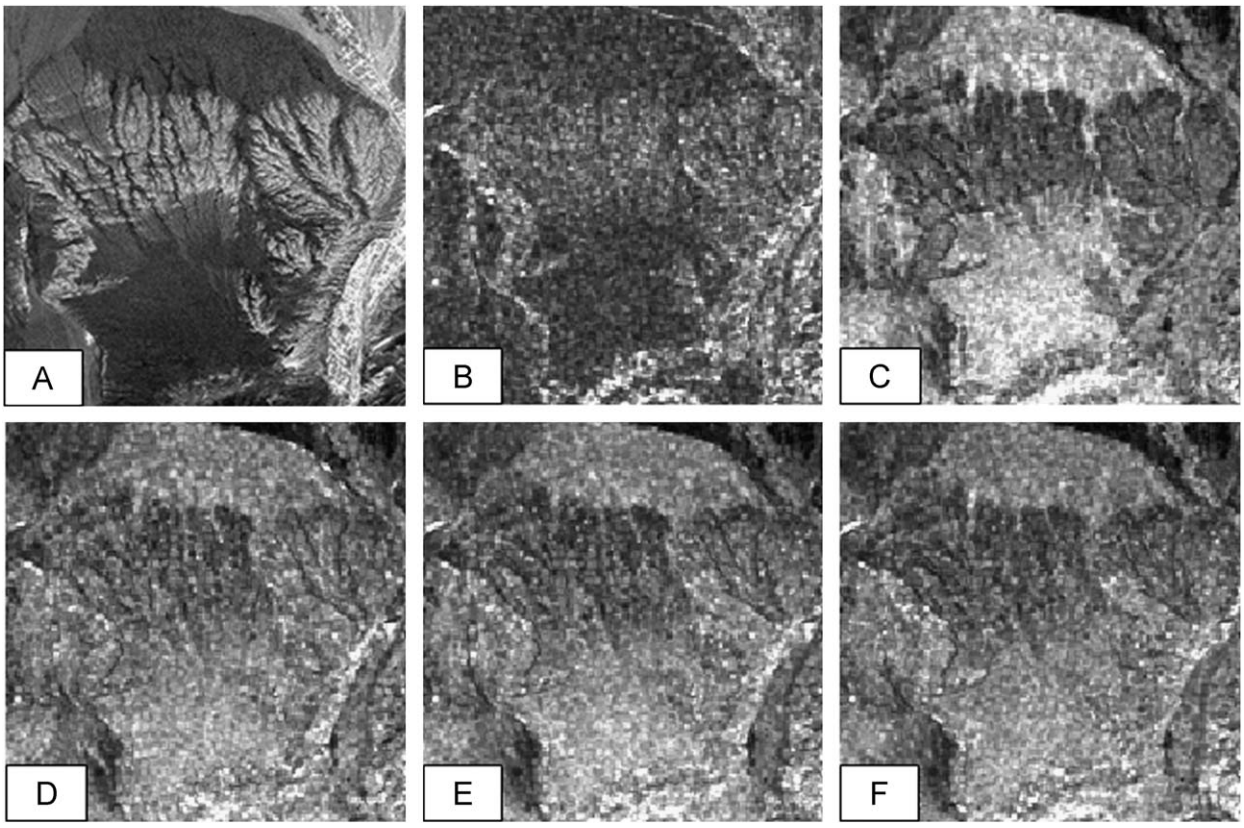

Fig. 10. SIR-C image and Lacunarity images obtained using different directionality (β) options. The lacunarity images were obtained with $r = 2$ and $w = 15$: (A) SIR-C image (17 km × 17 km) extracted from the original image (Courtesy NASA/JPL-Caltech); (B) non-directional lacunarity image; (C) lacunarity image with $\beta = 0^{\circ}$; (D) lacunarity image with $\beta = 45^{\circ}$; (E) lacunarity image with $\beta = 90^{\circ}$; and (F) lacunarity image with $\beta = 135^{\circ}$.

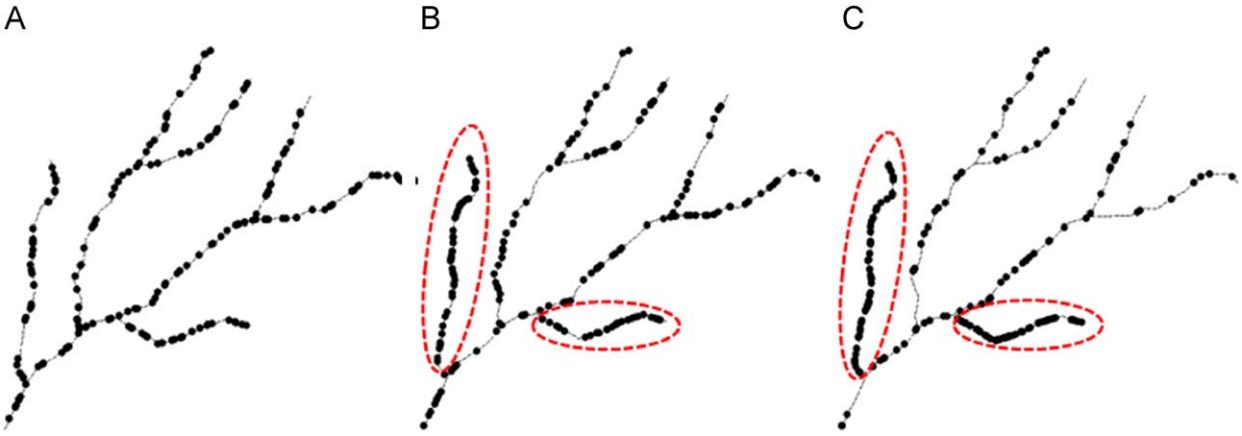

Fig. 11. Simulated 1D random point pattern (A) and clustered point patterns (B and C) on a drainage system. The total number of points is 200 for each pattern. The clusters are shown in ellipses.

points, it can be seen that the lacunarity of clustered patterns are higher than that of the random pattern in 3D, and that the greater the variations of gap sizes, the higher the lacunarity values in general. While it may be difficult to discriminate the patterns at one scale, these patterns can be separated at some other scales. This example shows the use of lacunarity in multiscale modeling.

Local lacunarity analysis can also be applied to 2D and 3D point patterns. For 3D point patterns, local lacunarity analysis basically calculates lacunarity values at a certain scale for the (x, y, z) points in the moving-window, and assign the lacunarity value to the center of each moving-window on the X–Y plane, thereby producing a 2D raster showing the lacunarity values. Fig. 14 shows a combined display of the clustered 3D points in Fig. 12D and their lacunarity image created using local lacunarity analysis. The lacunarity image in the backdrop is created using a 9×9 moving-window and a $3 \times 3 \times 3$ gliding-box. Other parameters are shown in the graphical interface in Fig. 6. It can be seen that the cluster in the central part of the dataset has higher lacunarity because this part has greater variations in gap sizes (small gaps in the cluster and large gaps outside the cluster).

Although examples of 2D point patterns are not shown in this paper, it is not difficult to imagine 2D as a special case of 3D, and expect similar results for 2D.

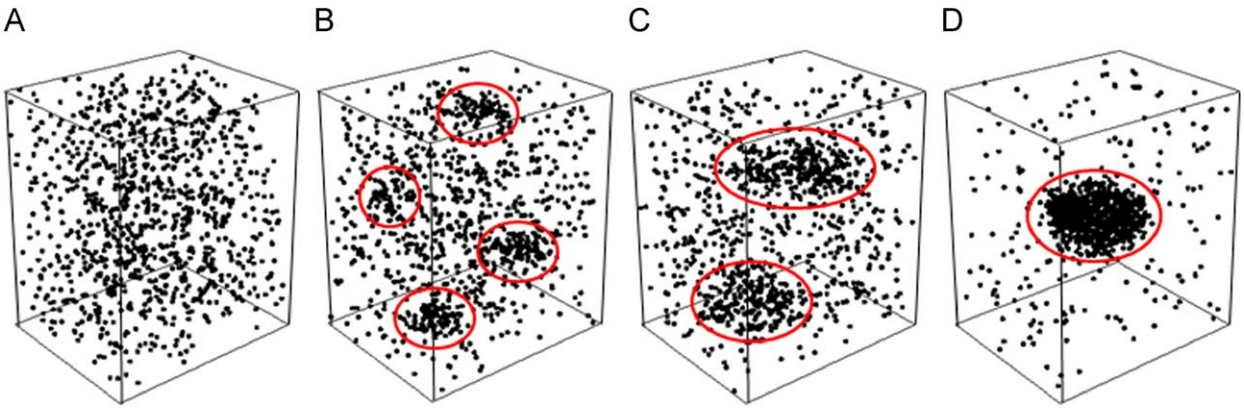

Fig. 12. Simulated random point pattern (A) and clustered point patterns (B, C and D) in 3D space. The total number of points is 1000 for each pattern. The clusters are shown in ellipses.

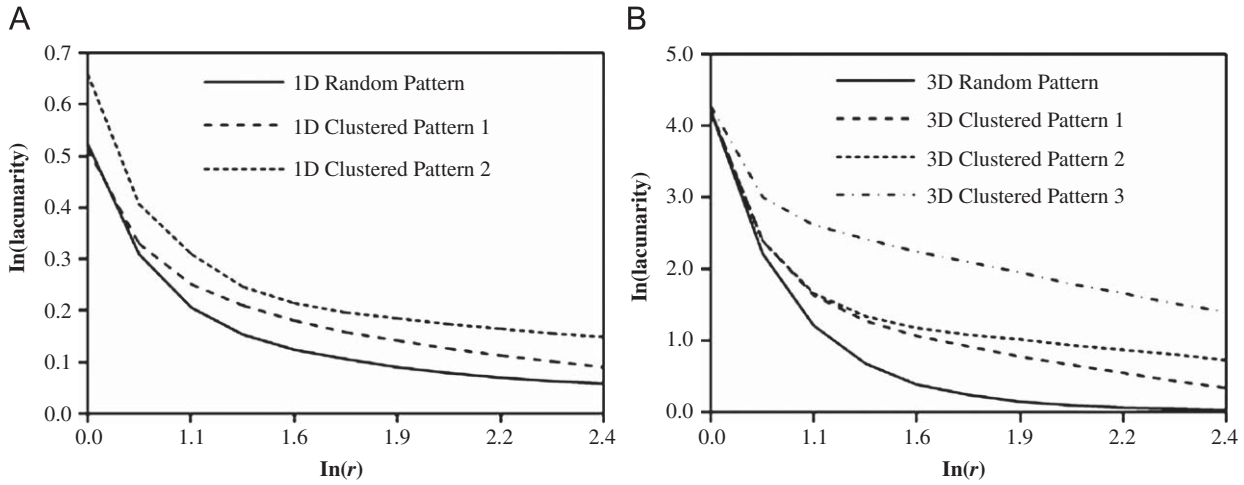

Fig. 13. Lacunarity curves for: (A) 1D point patterns and (B) 3D point patterns.

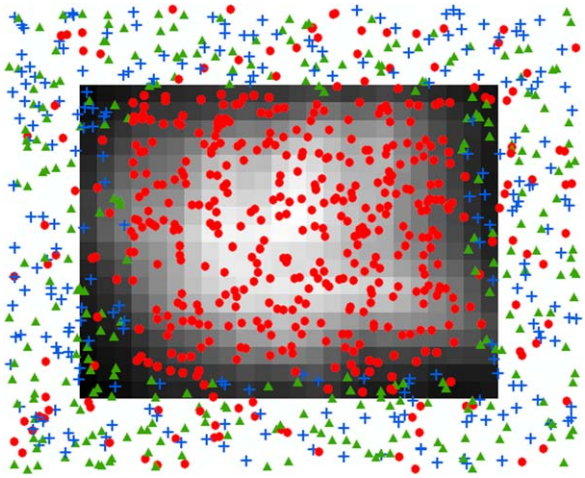

Fig. 14. Combined display of the clustered 3D points in Fig. 12D and their lacunarity image created using local lacunarity analysis at scale $r = 3$ (see GUI in Fig. 6 for other parameters). Z values of the points are presented using different symbols—cross (+): 0–5.5; dot (●): 5.5–9.0; and triangle (▲): 9.0–15.0.

5. Discussions

5.1. Options of lacunarity analysis

Similar to fractal dimension estimation, different methods of lacunarity estimation may generate different lacunarity measurements. It would be difficult to answer which methods are more accurate than the others, but it is possible to analyze which methods can provide more effective measurements in revealing the spatial heterogeneity of different patterns. In terms of grey-scale or binary options for lacunarity analysis, the choice depends on the data type and the research problem. Sometimes it is desirable to conduct lacunarity analysis using grey-scale datasets (for example, texture analysis of remotely sensed images), whereas in some applications the dataset needs to be converted to binary format for lacunarity analysis (for example, converting field observation data to binary format using certain thresholds). But there is no general rule on which option is better than the other.

5.2. Arrangement of polyline features and lacunarity of 1D points

Lacunarity analysis of 2D and 3D points only require a point feature class as input, and the order (or index) of the points does not affect the results. For 1D points, however, a polyline feature class is required in addition to the point feature class, so that the points can be rearranged into a 1D array. For moving objects such as people, vehicles, or animals, a unique trajectory for each object can be created based on the time stamp of each location, therefore there is no ambiguity in lacunarity calculation. However, for 1D points along a network such as a road network or drainage system, the arrangement of polyline features will affect the lacunarity of the 1D points.

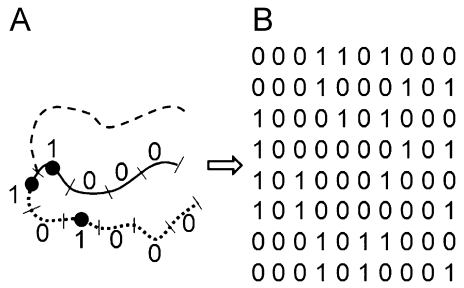

Fig. 15. Points on polyline segments (A) and possible combinations of 1D binary arrays (B).

Fig. 15A shows three polyline segments in a network. For clarity, the three segments are shown as a solid line, a dashed line, and a dotted line, respectively. Each segment has a *FromPoint* and a *ToPoint* for the starting location and the ending location of the segment. Take the solid and dotted segments for example (Fig. 15A), the two segments are divided into 10 linear pixels, with 1 for presence of points and 0 for absence of points. Since the *FromPoint* and *ToPoint* can be either on the left side or right side of each segment, and the order of the two segments can be different, there will be a total of eight possible combinations when the points are converted into 1D binary arrays (Fig. 15B). From Fig. 15B it can be seen that the size of the gaps (0's) can be quite different for the possible combinations, which means the lacunarity of the 1D points will be affected by the arrangement of the polyline segments. In other words, it might be difficult in such cases to find the *absolute* lacunarity values for the 1D points because of the effects of polyline arrangement, but the *relative* changes in lacunarity can still be useful in discriminating different 1D point patterns because the patterns are controlled by the same polyline feature class. This example suggests that: (1) the same polyline feature layer can be used when calculating lacunarity of different 1D point patterns on the polyline feature layer and (2) care should be taken when comparing lacunarity of different 1D point patterns controlled by different polyline feature classes (such as two different drainage systems).

6. Conclusion

The development and implementation of a lacunarity analysis extension for ArcGIS is presented along with several examples from raster datasets and point patterns. The extension provides global or local lacunarity analysis capabilities to meet the requirements of different applications. Because of the seamless integration with ArcGIS, the extension can use any raster data format supported by ArcGIS, and the results can be used by other ArcGIS functions. For raster datasets, problems of missing data, areas of interest, and directionality are taken into account, which can be very useful in real applications. The results from point patterns suggest that lacunarity can be used to test if a point pattern is random or clustered, and quantify the spatial heterogeneity at multiple scales. In general, the examples suggest that spatial patterns with different degrees of heterogeneity can be separated using lacunarity analysis, and that patterns that cannot be discriminated from each other at one scale can be separated at some other scales. The paper also suggests that care should be taken when comparing lacunarity of different 1D point patterns controlled by different polyline feature classes due to the uncertainty of feature arrangement. It is expected that the lacunarity analysis extension can provide useful tools for researchers in geosciences, environmental science, landscape ecology, geographic information science, and remote sensing, to conduct multiscale modeling of spatial patterns.

Acknowledgements

This research is supported in part by a University of North Texas (UNT) Faculty Summer Research Grant. The author would like to thanks NASA/JPL for providing the SIR-C image, and two anonymous reviewers for their helpful comments.

Appendix 1. Pseudo-code for generating 1D array for points on a network

```
Get polyline feature layer and point feature layer
Get polyline feature cursor pLineFCursor
Get point feature cursor pPointFCursor
Get first polyline:
Set pLineFeature = pLineFCursor.NextFeature
Do While Not pLineFeature Is Nothing
   Select points on pLineFeature
   Get first point:
   Set pPointFeature = pPointFCursor.NextFeature
   Do While Not pPointFeature Is Nothing
      Query point and distance to get DistanceAlong-
      Curve
      Accumulate DistanceAlongCurve for pPointFea-
      ture
      Put pPointFeature in 1D array using DistanceA-
      longCurve
      Move to next point:
      Set   pPointFeature = pPointFCursor.NextFea-
      ture
   Loop
   Accumulate length of 1D array
   Move to next polyline:
   Set pLineFeature = pLineFCursor.NextFeature
Loop
```

Appendix 2. Pseudo-code for 3D point conversion and analysis

```
Specify Z Range: Floor to Ceiling
Specify ZVoxelSize
Calculate NumberOfBands
For k = 0 To NumberOfBands - 1
   Z1 = Floor+k * ZVoxelSize
   Z2 = Floor+(k+1) * ZvoxelSize
   Select Points Where ZFieldValue > Z1 and ZField-
   Value < = Z2
   Convert Selected Points to RasterBand
   Add RasterBand To InputBandCollection
Next k
For k = 0 To NumberOfBands - 1
   Get RawPixel from InputBandCollection.Item(k)
   Get InputPixelBlock(i, j) from RawPixel
   Get  Input3DArray(i,  j,  k)  from  InputPixel-
   Block(i, j)
Next k
Calculate Lacunarity of Moving-windows in Input3-
DArray.
Assign Lacunarity Values to OutputPixelBlock.
Write Output Pixel Block to the Output Raster.
```

Appendix 3. Pseudo-code for partitioning large dataset into blocks

```
Determine BlockSize
ValidBlockHeight = BlockSize
   - WindowSize+1
BlockLeft = 0
BlockTop = 0
BlockWidth = RasterWidth
BlockIndex = 0
AllBlocksAreProcessed = False
Do While Not
   AllBlocksAreProcessed
                              BlockTop = BlockIndex *
                              ValidBlockHeight
                              If BlockTop = 0 And BlockSize > =
                              RasterHeight Then
                                BlockHeight = RasterHeight
                                AllBlocksAreProcessed = True
                              ElseIf BlockTop > = RasterHeight
                              - BlockSize - WindowSize Then
                                BlockHeight = RasterHeight-
                              BlockTop
                                AllBlocksAreProcessed = True
                              Else
                                BlockHeight = BlockSize
                              End If

                              (1) Initialize input pixel block
                              using BlockWidth and BlockHeight.
                              (2) Read input pixel block based on
                              BlockLeft and BlockTop.
                              (3) Calculate lacunarity of
                              moving-windows in the block.
                              (4) Assign lacunarity values to the
                              output pixel block.
                              (5) Write output pixel block to the
                              output raster.
                              (6) Move to next block:
                              BlockIndex = BlockIndex+1.
Loop
```

Appendix 4. Sample output text file from global lacunarity analysis

Box_Size	Lacunarity	ln(Box_Size)	ln(Lacunarity)
1	524.0872	0.0000	6.2617
2	65.8496	0.6931	4.1874
3	20.1982	1.0986	3.0056
4	9.1039	1.3863	2.2087
5	5.1460	1.6094	1.6382
6	3.3852	1.7918	1.2194
7	2.4926	1.9459	0.9133
8	1.9934	2.0794	0.6899
9	1.6961	2.1972	0.5283
10	1.5038	2.3026	0.4080
11	1.3760	2.3979	0.3192
12	1.2886	2.4849	0.2536
13	1.2259	2.5649	0.2036
14	1.1797	2.6391	0.1653
15	1.1444	2.7081	0.1349
16	1.1180	2.7726	0.1116
17	1.0969	2.8332	0.0925
18	1.0802	2.8904	0.0772
19	1.0675	2.9444	0.0653

Appendix 5. Supporting Information

Supplementary data associated with this article can be found in the online version at doi:10.1016/j.cageo.2009.04.001.

References

Allain, C., Cloitre, M., 1991. Characterizing the lacunarity of random and determined fractal set. Physics Review A 44, 3552–3558.

Boots, B.N., Getis, A., 1988. Point Pattern Analysis. Sage Publications, Newbury Park, CA.

Brodatz, P., 1966. Texture: A Photographic Album for Artists and Designers. Dover, New York.

Chun, H.C., Giménez, D., Yoon, S.W., 2008. Morphology, lacunarity and entropy of intra-aggregate pores: aggregate size and soil management effects. Geoderma 145, 83–93.

Dell'Acqua, F., Gamba, P., 2006. Discriminating urban environments using multi-scale texture and multiple SAR images. International Journal of Remote Sensing 27, 3797–3812.

Dong, P., 2000. Test of a new lacunarity estimation method for image texture analysis. International Journal of Remote Sensing 21, 3369–3373.

Dong, P., Leblon, B., 2004. Rock unit discrimination on Landsat TM, SIR-C and Radarsat images using spectral and textural information. International Journal of Remote Sensing 25, 3745–3768.

ESRI, 2004. ArcGIS 9—ArcGIS Desktop Developer Guide, 329 pp.

Frazer, G.W., Wulder, M.A., Niemann, K.O., 2005. Simulation and quantification of the fine-scale spatial pattern and heterogeneity of forest canopy structure: a lacunarity-based method designed for analysis of continuous canopy heights. Forest Ecology and Management 214, 65–90.

Gefen, Y., Aharony, A., Mandelbrot, B.B., 1984. Phase transitions on fractals: III. Infinitely ramified lattices. Journal of Physics A: Mathematical and General 17, 1277–1289.

Guo, H., Liao, J., Wang, C., Wang, C., Farr, T.G., Evans, D.L., 1997. Use of multifrequency, multipolarization Shuttle Imaging Radar for volcano mapping in the Kunlun Mountains of Western China. Remote Sensing of Environment 59, 364–374.

Hay, G.J., Castilla, G., Wulder, M.A., Ruiz, J.R., 2005. An automated object-based approach for the multiscale image segmentation of forest scenes. International Journal of Applied Earth Observation and Geoinformation 7, 339–359.

Henebry, G.M., Kux, H.J.H., 1995. Lacunarity as a texture measure for SAR imagery. International Journal of Remote Sensing 16, 565–571.

Lang, S., Burnett, C., Blaschke, T., 2004. Multiscale object-based image analysis a key to the hierarchical organisation of landscapes. Ekologia-Bratislava 23, 148–156.

Lin, B., Yang, Z.R., 1986. A suggested lacunarity expression for Sierpinski carpets. Journal of Physics A: Mathematical and General 19, L49–L52.

Louie, M.M., Kolaczyk, E.D., 2006. A multiscale method for disease mapping in spatial epidemiology. Statistics in Medicine 25, 1287–1306.

Lucieer, A., Stein, A., 2005. Texture-based landform segmentation of LiDAR imagery. International Journal of Applied Earth Observation and Geoinformation 6, 261–270.

Malhi, Y., Román-Cuesta, R.M., 2008. Analysis of lacunarity and scales of spatial homogeneity in IKONOS images of Amazonian tropical forest canopies. Remote Sensing of Environment 112, 2074–2087.

Mandelbrot, B.B., 1982. The Fractal Geometry of Nature. Freeman, San Francisco, CA.

Miranda-Martinez, E., Oleschko, K., Parrot, J.F., Castrejon-Vacio, F., Hind, T., Brambila-Pazl, F., 2006. Porosity in naturally fractured media: a fractal classification. Revista Mexicana de Ciencias Geologicas 23, 199–214.

Mygal, V.P., Phomin, A.S., 2006. The multiscale spectral and spatial character of photoresponse in CdZnTe crystals. Technical Physics Letters 32, 484–486.

Myint, S.W., Lam, N., 2005. A study of lacunarity-based texture analysis approaches to improve urban image classification. Computers, Environment and Urban Systems 29, 501–523.

Pasher, J., King, D.J., 2006. Landscape fragmentation and ice storm damage in eastern Ontario forests. Landscape Ecology 21, 477–483.

Plotnick, R.E., Gardner, R.H., O'Neill, R.V., 1993. Lacunarity indices as measures of landscape texture. Landscape Ecology 8, 201–211.

Plotnick, R.E., Gardner, R.H., Hargrove, W.W., Prestegaard, K., Perlmutter, M., 1996. Lacunarity analysis: a general technique for the analysis of spatial patterns. Physical Review E 53, 5461–5468.

Rankey, E.C., 2002. Spatial patterns of sediment accumulation on a Holocene carbonate tidal flat, northwest Andros Island, Bahamas. Journal of Sedimentary Research 72, 591–601.

Ranson, K.J., Sun, G., 1997. An evaluation of AIRSAR and SIR-C/X-SAR images for mapping northern forest attributes in Maine, USA. Remote Sensing of Environment 59, 203–222.

Ripley, B., 1988. Statistical Inference for Spatial Processes. Cambridge University Press, Cambridge.

Sarkar, N., Chaudhuri, B.B., 1992. An efficient approach to estimate fractal dimension of textural images. Pattern Recognition 25, 1035–1041.

Shoshany, M., Even-Paz, A., Bekhor, S., 2007. Evolution of clusters in dynamic point patterns: with a case study of Ants' simulation. International Journal of Geographical Information Science 21, 777–797.

Vigiak, O., van Loon, E., Sterk, G., 2006. Modelling spatial scales of water erosion in the West Usambara Mountains of Tanzania. Geomorphology 76, 26–42.

Voss, R., 1986. Random fractals: characterization and measurement. In: Pynn, R., Skjeltorp, A. (Eds.), Scaling Phenomena in Disordered Systems. Plenum Press, New York, pp. 37–48.

Vvedensky, D.D., 2004. Multiscale modelling of nanostructures. Journal of Physics-Condensed Matter 16, MDXXXVII–MDLXXVI.

Watts, D.J., Muhamad, R., Medina, D.C., Dodds, P.S., 2005. Multiscale, resurgent epidemics in a hierarchical metapopulation model. Proceedings of

the National Academy of Sciences of the United States of America 102, 11157–11162.
Wu, X.B., Thurow, T.L., Whisenant, S.G., 2000. Fragmentation and changes in hydrologic function of tiger bush landscapes, south-west Niger. Journal of Ecology 88, 790–800.
Wu, Y.G., Wang, N.M., Rutchey, K., 2006. An analysis of spatial complexity of ridge and slough patterns in the Everglades ecosystem. Ecological Complexity 3, 183–192.
Xu, Y., Burton, P.W., 1997. Microearthquake swarms: scaling and lacunarity. Geophysical Journal International 131, F1–F8.